Journal of Sound and Vibration (1997) **203**(4), 621–639

SIMULATION OF TWO-DIMENSIONAL SQUEEZE FILM AND SOLID CONTACT FORCES ACTING ON A HEAT EXCHANGER TUBE†

T. ZHOU

CIM Lab, Dept. of Mechanical Engineering, University of Toronto, Toronto, Ontario M5S 3G8, Canada

AND

R. J. ROGERS

Department of Mechanical Engineering, University of New Brunswick, Fredericton, N.B. E3B 5A3, Canada

(*Received* 18 *September* 1995, *and in final form* 11 *December* 1996)

Based on a short-length cylindrical squeeze film model, a simplified two-dimensional dynamic model for the interaction of a heat exchanger tube and its support, with transitions to and from solid contact, has been developed. The model includes estimations of the tube/support deflection, the effects of the surface roughnesses and tube/support inclination. A test computer code based on the model has been developed which calculates the normal and tangential squeeze film forces and solid contact forces acting on the tube with large amplitude arbitrary motions. As well, the code has been extended to simulate a mass with six degrees of freedom. The model and algorithm have been verified by numerical analysis and comparisons. The VIBIC finite element computer code which simulates the dynamic response of a heat exchanger tube as it impacts and rubs against its supports has been improved and updated by implementing the test code into it. The simulation results appear reasonable.

1. INTRODUCTION

The avoidance of flow-induced vibration damage is a major concern of designers and operators of shell and tube heat exchangers. The turbulent flow of the shell-side fluid around the tubes results in tube vibration. This kind of vibration can lead to large amplitude motions or large eccentricities of the tubes in their support plate holes (which are larger than the tube outside diameters in order to allow for assembly and thermal expansion). Fluid forces called squeeze film forces occur within the clearance spaces when the tubes approach their supports and significant solid contact forces may occur when the tubes' responses exceed the clearance. The contact forces, especially tangential solid contact forces, can lead to excessive fretting wear of the tubes. In order to predict the wear damage, it is necessary to simulate the vibration patterns and calculate these forces. To do this, finite element computer codes such as VIBIC (for Vibration of Beams with Intermittent Contacts) have been developed [1, 2]. To improve the modelling, a better transition to and from the solid contact model is required.

†Also presented with permission at the Symposium on Flow-Induced Vibration—1996, Joint ASME PVP/ICPVT-8 Conference, July 21–26, Montreal, Canada [24].

0022–460X/97/240621 + 19 $25.00/0/sv960870

Squeeze film forces have long been of considerable interest. These forces occur between two surfaces which are separated by fluid and have relative movement mainly in the normal direction. Several theoretical models [3–7] can be found to calculate the squeeze film forces for cylindrical geometries.

In a circular cylindrical squeeze film, there are normally two kinds of forces: one is caused by the viscosity of the fluid when it is squeezed to flow within the fluid film and the other one is caused by the mass of the fluid when it is accelerated. The two kinds of forces are named viscous (or damping) force and inertia force, respectively. Furthermore, there are several sources for the fluid to obtain acceleration, such as the acceleration of the cylinder, the changes in the velocity direction, as well as centripetal and Coriolis accelerations. The inertia force is resolved accordingly into several components named unsteady, convective, centripetal and Coriolis inertia forces.

San Andres and Vance [3] obtained expressions for the unsteady inertia and damping coefficients of finite length squeeze film dampers. Assuming small vibration amplitude, as done by many researchers, they neglected the convective fluid inertia force which plays a relatively important role for large amplitude motions or large initial eccentricities of the tube. Some researchers have considered this effect in their theory and experiments [4, 5]. When a tube has arbitrary two-dimensional motions, the centripetal and Coriolis accelerations need to be considered. The corresponding inertia forces have been recently formulated by several researchers [6, 7].

A suitable squeeze film model for arbitrary two-dimensional, large amplitude or large eccentricity tube motions was developed by Lu and Rogers [7]. They formulated the instantaneous squeeze film force for arbitrary tube motions based on a short squeeze film model. All the terms of the force components are position-dependent and non-linear. The theoretical model was evaluated using experimental data from a finite length squeeze film. The comparison shows fair agreement between the theoretical model and experimental results [7].

The solid contact model must include material elastic and damping forces, as well as the friction force. Since neither a heat exchanger tube nor its supports are solid, it is assumed that for small loads the load–deflection relationship can be treated as linear. This assumption turns Hertzian contact theory [8] into Hooke's law which is based on modelling elastic bodies with equivalent linear springs. In order to demonstrate the loss of energy due to the plastic deformation involved during the impact, a coefficient of restitution is introduced and studied by many researchers e.g., references [9, 10]. Hunt and Crossley [9] used the classical definition of coefficient of restitution and obtained a non-linear material damping coefficient. The new model changed the half-ellipse hysteresis loop produced by the combination of linear damping and spring to a closed loop which comes to a sharp point at the origin and seems more reasonable. Physical experiments have confirmed their postulation.

Lewis and Rogers [11, 12] did some experiments and simulations of oblique impact. During contact the friction coefficient was observed to rise to a "plateau" value and then decline to zero as contact was lost. The plateau value was found to be independent of impact velocity and a bilinear function of impact angle.

When the sliding velocity changes direction or when it is very small, sticking or adherence may physically occur between the two contacting bodies. A sticking friction model which can detect the sticking phenomenon of the tube and calculate the striking friction force has been recently developed and implemented into VIBIC by Tan and Rogers [13, 14]. In this model, sticking is considered to occur when the sliding velocity is lower than a given small velocity providing that the sticking friction force, which is obtained from the force equilibrium, is less than the maximum friction force, which is obtained from the

Coulomb law. This model gives good numerical results for oblique impact and sliding reversal cases.

Because the squeeze film model is very different from the solid contact model, difficulties exist in any transition model which simulates tube motions and calculates the forces acting on the tube when the tube goes from squeeze film to solid contact with a support and then bounces back. Theoretically, a squeeze film cannot be broken if perfect geometries and rigid bodies are assumed. However, this does not happen in real equipment. The tube does break the squeeze film and becomes involved in solid contact with the support, especially for a low viscosity medium such as water. In order to combine these two kinds of models together and smoothly switch the calculation of forces from the squeeze film model to the solid contact model and vice versa, a robust transition model is required. The development of a dynamic transition squeeze film model and its implementation into VIBIC are the objectives of this work. The present model extends an earlier primitive model [25].

2. SQUEEZE FILM AND SOLID CONTACT MODELS

The instantaneous squeeze film force, which is related to the instantaneous position, velocity and acceleration of the tube within its support hole, was formulated based on a 2π short length, cylindrical squeeze film model [7]. The force is resolved into normal and tangential components. As shown in Figure 1, the co-ordinates and directions are defined as follows: the origin point is located at the centre of the sleeve; the normal vector is a unit vector from the sleeve centre to the instantaneous tube centre; and the tangential vector is a unit vector perpendicular to the normal vector. Y- and Z-axes are the global Cartesian co-ordinates on which the tube position or motions in its support hole are described. The angle from the positive direction of the Y-axis to the normal direction is denoted as the instantaneous angular displacement Ψ of the tube centre. The components of the squeeze film force are given by [7]

$$\frac{F_{sqn}}{L^3R} = -\mu\frac{\pi(1+2\varepsilon^2)}{C_r^2\gamma^5}\dot{\varepsilon} - \rho\frac{\pi(1-\gamma)}{6\varepsilon^2\gamma}\ddot{\varepsilon} - \rho\frac{3\pi}{20\varepsilon^3}\left(2-\frac{2-3\varepsilon^2}{\gamma^3}\right)\dot{\varepsilon}^2$$

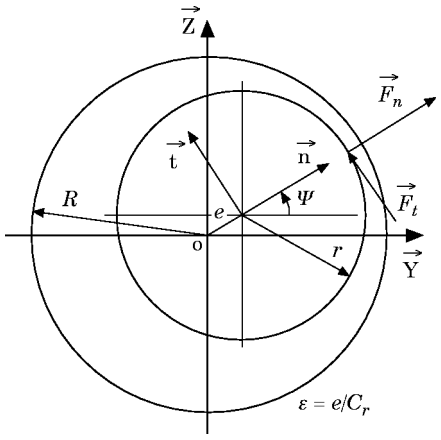

Figure 1. Co-ordinate system and unit vectors.

$$+\rho\,\frac{\pi(1-\gamma)}{6\varepsilon^2\gamma}\left(1-\frac{9}{10}(1-\gamma)\right)\varepsilon\dot{\Psi}^2,$$

$$\frac{F_{sqt}}{L^3R}=-\mu\,\frac{\pi}{C_r^2\gamma^3}\,\varepsilon\dot{\Psi}-\rho\,\frac{\pi(1-\gamma)}{6\varepsilon^2}\,\varepsilon\ddot{\Psi}-\rho\,\frac{\pi(1-\gamma)}{3\varepsilon^2}\left(1+\frac{9}{10}\,\frac{(1-\gamma)}{\upsilon}\right)\varepsilon\dot{\Psi}, \tag{1}$$

where $\gamma=\sqrt{1-\varepsilon^2}$ and $\varepsilon=e/C_r$ is the non-dimensional instantaneous eccentricity and is an important factor in calculating the squeeze forces. See the nomenclature for variable definitions.

As the tube approaches very near the support surface ($\varepsilon>0{\cdot}95$), the squeeze film will dissipate and solid contact between the tube and the support will occur. During the contact, two solid contact forces exist along the normal and tangential direction which are mainly due to material stiffness and friction, respectively. The forces are formulated as

$$F_{ctn}=-KX_w-1{\cdot}5\beta KX_w\dot{X}_w, \tag{2}$$

$$F_{ctt}=-\text{sign}\,(v_t)\mu_kF_{ctn},\quad\text{for slipping;}\qquad F_{ctt}=F_{sti},\quad\text{for sticking;} \tag{3a, b}$$

where X_w is the deformation of the contact surfaces and K is the combined normal stiffness of tube and support. The coefficient of material damping, β, is based on the contact materials and impact velocity [9]. For mild steel, a value of β can be estimated as $0{\cdot}3$ s/m at low velocities by extrapolating the curves in Goldsmith [15].

Equation (3a) is the classical Coulomb friction model, which is used when the tube is in a slipping state. Because of the sharp discontinuity in the frictional force of the Coulomb model when v_t reverses direction, if v_t is very small, this classical model can cause numerical chatter of the frictional force. As well, when v_t reverses direction or when it is very small, sticking or adherence may physically occur. In order to overcome the weakness of the Coulomb model, a new friction model (3a, b) including sticking-slipping motions has been developed [13] and is used in this work. In equation (3b), F_{sti} is the sticking friction force which balances all other forces acting on the tube. When v_t is lower than a given limiting velocity, v_c, and if the sticking friction force is less than the maximum static friction force, the tube is considered to be in a sticking state and is maintained in the sticking state by F_{sti}. Once this sticking friction force is larger than the maximum friction force, the sticking state is broken and the state of the tube will change from sticking to slipping, where the classical model (3a) can be employed to calculate the slipping friction force.

Lewis and Rogers [11, 12] obtained a bilinear function of impact angle for the friction coefficient:

$$\mu_k=\mu_0\theta_i/40,\quad\text{for } 0^\circ<\theta_i<40^\circ;\qquad\mu_k=\mu_0,\quad\text{for } \theta_i\geqslant 40^\circ; \tag{4}$$

where θ_i is the impact angle measured from the normal direction. Recent unpublished simulations of their experiments have shown that the reduction in the apparent coefficient of friction is not due to sticking since the tangential velocity of the contact point does not approach zero.

3. DYNAMIC MODEL OF TRANSITIONS TO AND FROM SOLID CONTACT

The fluid and solid models have been obtained separately. They are totally different concepts. When the tube vibrates at large amplitude or large initial eccentricity in its support hole, both phenomena may occur physically. Therefore both squeeze and solid contact forces have to be calculated simultaneously.

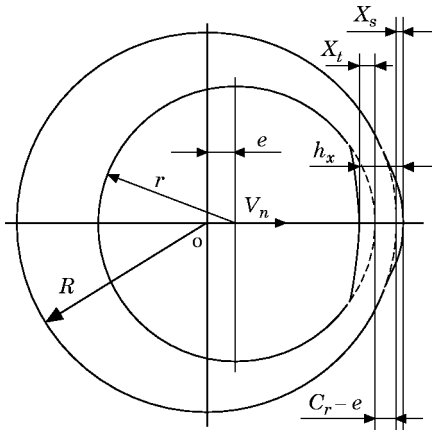

Figure 2. Squeeze film and deflections of tube/support.

3.1. WALL DEFLECTION

When the normal velocity of the tube v_n is positive, a squeeze film occurs between the surfaces of the tube and the support. As the tube approaches very near the support, the normal squeeze force becomes quite large and tends to deform the tube and the support walls. The deflections increase the minimum film thickness as shown conceptually in Figure 2. At the same time, the deflections also influence the actual velocity and acceleration of the changes in the minimum squeeze film thickness.

By not considering surface deflections, the minimum film thickness is $h = C_r - e$, where C_r is the radial clearance between tube and support, and e is the instantaneous radial displacement of the tube centre.

With the elastic tube and support deflections, the minimum film thickness becomes

$$h_x = C_r - e + X_t + X_s = C_r - e + X_w, \tag{5}$$

where X_t and X_s are the deflections of tube and support, respectively; $X_w = X_t + X_s =$ combined deflection. Since generally the stiffness of the support is much greater than that of the tube, X_s can be neglected compared to X_t so that $X_w \approx X_t$.

The concept of tube/support deflection is the core of the dynamic model. The normal direction squeeze force will itself cause some local deflection. The elastic and damping forces in equation (2) must therefore balance the normal squeeze force:

$$KX_w + \tfrac{3}{2}\beta K X_w \dot{X}_w = F_{sqn}(e, \dot{e}, \ddot{e}), \tag{6}$$

where $F_{sqn}(e, \dot{e}, \ddot{e})$ is the squeeze film normal force in equation (1) which is a function of the displacement, velocity and acceleration of the tube. The value X_w solved from equation (6) is substituted into equation (2) to get a smooth change when the calculation is switched from fluid to solid.

As the minimum film thickness has been changed from $C_r - e$ to $C_r - e + X_w$ caused by the deflection, the squeeze film force acting on the tube will be affected. In equation (1), the value of displacement e (or ε) in fact indicates the minimum film thickness because the total squeeze force is mainly caused by the high pressure around the region of the minimum film thickness. Thus one can re-evaluate e as

$$e_e = e - X_w, \tag{7}$$

where e_e is called "effective" displacement.

Furthermore, for the same reason, the normal velocity and acceleration of the tube also can be re-evaluated as

$$\dot{e}_e = \dot{e} - \dot{X}_w, \qquad \ddot{e}_e = \ddot{e} - \ddot{X}_w. \tag{8}$$

Then the force balance equation (6) becomes

$$KX_w + \tfrac{3}{2}\beta K X_w \dot{X}_w = F_{sqn}(e_e, \dot{e}_e, \ddot{e}_e), \tag{9}$$

where $(e_e, \dot{e}_e, \ddot{e}_e)$ are the "effective" values.

3.2. EFFECTIVE RADIAL DIMENSIONS

One hopes not to calculate the squeeze film force when ε is quite large because of the theoretical weakness of dividing by zero when $\varepsilon \to 1$. In practice, the tube cannot reach the point of $\varepsilon = 1$ without solid contact because of imperfect engineering equipment. This leads to the concept of effective dimensions which allows solid contact before ε reaches 1.

As shown in Figure 3, the inclination of the tube relative to its support surface always exists due to angular misalignment and tube rocking motions. This causes solid contact before the minimum film thickness, h_x, goes to zero. One has

$$h_s = (L/2) \tan \alpha, \tag{10}$$

where h_s is the clearance at the support centre when a tube with slope α contacts the edge of the support. A typical value for α is $0{\cdot}05^\circ$ [16]. In practical terms, h_s decreases the effective dimension of the support hole (i.e., R).

As shown in Figure 4, when the tube approaches very near the support, solid contact occurs at some roughness peaks before h_x goes to zero because of the existence of the surface roughness of tube/support. h_r is defined as the sum of the r.m.s. roughnesses of the tube/support surfaces. For a broached or reamed hole and a typical tube, $h_r = 3\ \mu\text{m}$ is used [17]. The consideration of roughness leads to the concept of a transition zone where combined calculations of fluid and solid forces are carried out.

3.3. DYNAMIC MODEL AND TRANSITION CRITERIA

Considering the deflection X_w, tube inclination h_s and surface roughness h_r, as well as squeeze film normal force F_{sqn} and material resistance force, a simplified dynamic model as shown in Figure 5 was obtained, where c is the non-linear material damping coefficient $(1{\cdot}5\beta K X_w)$. Material elastic and damping forces compose the material resistance force.

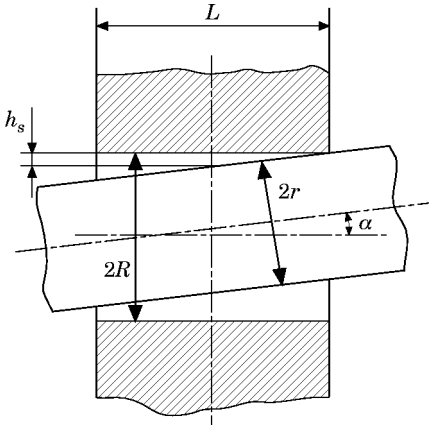

Figure 3. Inclination of tube in its support.

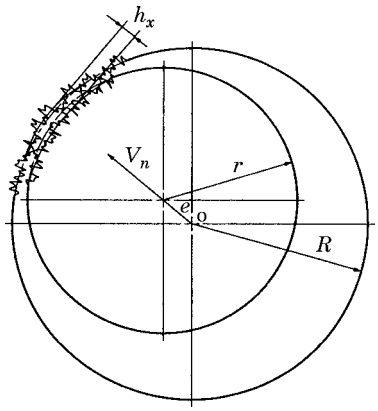

Figure 4. Surface roughnesses of tube/support.

In order to determine when solid contact will occur, according to this dynamic model, the following criteria and calculations are used:

(1) If $h_x \geqslant h_r + h_s$, there is no solid contact at all. The tube is separated thoroughly from the support by fluid. This stage is the fully squeeze zone. At this time, the squeeze film model is used so that F_{sqn} and F_{sqt} are calculated using equation (1) with effective values $(e_e, \dot{e}_e, \ddot{e}_e)$.

(2) If $h_s < h_x < h_r + h_s$, the tube is in the roughness zone and the squeeze film is dissipated by some roughness peaks in the region around the minimum film thickness area. Slight contact occurs now. At this stage, both fluid and solid forces exist and neither of them is dominant. This stage is considered as the transition zone which is used to gradually switch from fluid calculation to solid calculation. Since the wall deflection X_w is calculated based on the normal force balance equation, the normal fluid force is equal to the normal solid force whenever X_w is calculated from equation (9). The normal force can be switched smoothly from the fluid model to the solid model when the tube comes into the transition zone because at this moment, the deflection obtained from equation (9) is equal to $(e - C_r) + (h_r + h_s)$ which is the same as the solid wall deflection without squeeze force as seen in Figure 5. Thus only the normal solid force is taken as the total normal force during the transition zone. However, for the tangential force, both fluid and solid forces exist. The tangential squeeze force is hardly affected by the tiny contact

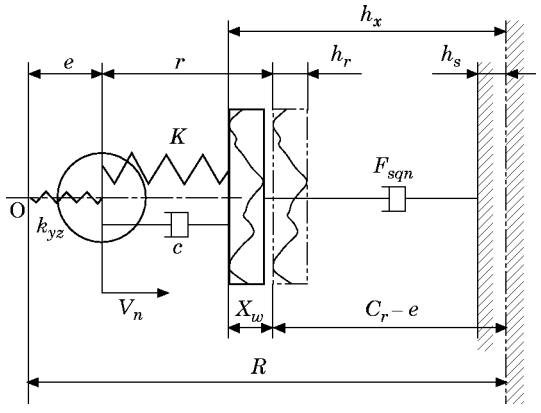

Figure 5. Dynamic model of squeeze film and deflection

area so that it always plays a significant role which cannot be taken over by solid friction. In order to gradually take the solid friction force into consideration in the total tangential force, a blended calculation of fluid and solid forces is used at this stage. The calculation is formulated as

$$F_n = F_{ctn}, \qquad F_t = F_{sqt} + pF_{ctt}, \tag{11}$$

where F_{sqt} is defined in equation (1) and p is a weighting factor used to show the proportion of solid friction force in the total tangential force, valued between 0 and 1, and is adapted from Oden and Martins [18]:

$$p(h_x) = \tfrac{1}{2} + \tfrac{1}{2}(2 - |g(h_x)|)g(h_x), \tag{12}$$

where $g(h_x) = (2h_x - 2h_s - h_r)/h_r$.

(3) If $h_x \leqslant h_s$, it is considered that real solid contact occurs at the corner of the sleeve as seen in Figure 3. This stage is the fully contact zone. At this time, the contact normal force is dominant while squeeze and contact tangential forces have full contributions. The following calculations are used:

$$F_n = F_{ctn}, \qquad F_t = F_{sqt} + F_{ctt}, \tag{13}$$

where F_{sqt} is obtained from equation (1) in which the eccentricity is kept as a constant value $e = C_r - h_s$.

Once the tube gets into contact (i.e., in transition or fully contact zones), the solid deflection of the tube/support walls is no longer calculated by equation (9) but by

$$X_w = (e - C_r) + (h_r + h_s). \tag{14}$$

3.4. SUCTION FORCE

When the normal velocity of the tube is negative ($v_n < 0$), the tube is either losing solid contact or moving away from a support surface. The same criteria described above are used. Instead of the "squeeze" force, a suction force caused by the negative gauge pressures occurs in the vicinity of the minimum film thickness. When $C_r - e \geqslant h_r + h_s$, there are no solid forces so that the fluid suction force is dominant. This force acts to slow down the wall of the tube and causes the equivalent spring to increase the distance between the tube centre and the tube wall. The same equation (9) is used to calculate the wall deflection. However, the suction force cannot be as large as the squeeze normal force because the negative gauge pressure at most can only be one negative atmosphere. In fact, if the absolute pressure becomes lower than the liquid vapor pressure, the liquid film ruptures and a cavity is formed in this negative gauge pressure region. Within the cavity, the pressure is nearly constant and almost equal to absolute zero pressure [19]. In order to have an estimation for the maximum suction force, a very rough assumption is considered. It is assumed that the cavity occurs all over the entire negative pressure area. In lubrication terms, the 2π film becomes a π film. This assumption probably over-estimates the maximum suction force.

With the above assumption, the maximum suction force can be obtained roughly by the integral

$$F_{max} \approx \int_{-\pi/2}^{\pi/2} (P_{oper} - P_{vap}) rL \cos\theta \, \mathrm{d}\theta = 2(P_{oper} - P_{vap}) rL, \tag{15}$$

where P_{oper} is the operating pressure and P_{vap} is the liquid vapor pressure.

4. MODEL IMPLEMENTATION INTO TEST CODE AND VIBIC

To simulate the dynamic response of a heat exchanger tube as it impacts and rubs against its supports, a finite element computer code named VIBIC has been developed [1, 2]. The present work is intended to improve the transition to and from solid contact model. This section explains how the model is carried out numerically. For ease of testing, it was implemented into a small test code first before implementing into VIBIC.

4.1. CALCULATION OF WALL DEFLECTION

In order to get a smooth transition when the tube gets into solid contact from the squeeze film or loses contact, a dynamic model which considers the wall deflections of the tube/support has been developed and shown in Figure 5. The governing equation for the combined deflection X_w is given by equation (9).

It can be seen that equation (9) is an implicit equation: the left side is a function of X_w and so is the right side. Since the right side of the equation is a very complex function of X_w expressed by equation (1) (almost all the variables are affected by X_w), it is not easy to get an explicit solution of X_w. The Newton–Raphson iteration method is chosen in the computer code to obtain X_w from equation (9):

$$X_w(m+1) = X_w(m) - F(X_w(m))/F'(X_W(m)), \tag{16}$$

where $F(X_w)$ is an iterative function of X_w and formulated as

$$F(X_w) = KX_w + \tfrac{3}{2}\beta K X_w \dot{X}_w - F_{sqn}(e_e, \dot{e}_e, \ddot{e}_e). \tag{17}$$

$F'(X_w)$ is its derivative with respect to X_w and is evaluated numerically in the code. After X_w is obtained, $\dot{X}_w$ and $\ddot{X}_w$ in equation (8) are calculated numerically by using simple backward differences of deflection and velocity, respectively.

4.2. OTHER IMPLEMENTATION CONSIDERATIONS

The dynamic model introduced in the last section has solved the difficulty of the squeeze film calculation in equation (1) when $\varepsilon \to 1$. For the other extreme, $\varepsilon \to 0$, a problem still exists. As shown in equation (1), the inertia terms contain ε^2 or ε^3 in the denominators. These terms become inaccurate when $\varepsilon \to 0$. The limits of equation (1) were obtained:

$$\lim_{\varepsilon \to 0} F_{sqn}/L^3R = -(\mu\pi/C_r^3)v_n - (\rho\pi/12C_r)a_n,$$

$$\lim_{\varepsilon \to 0} F_{sqt}/L^3R = -(\mu\pi/C_r^3)v_t - (\rho\pi/12C_r)a_t. \tag{18}$$

It is shown that (v_n, v_t) or (a_n, a_t) have exactly the same influence on the squeeze film forces. This means the normal and tangential directions have no difference when $\varepsilon \to 0$, which is physically true. The squeeze force equations can therefore be written directly as Y and Z force components for very small values of ε.

Using the models and algorithm described above, a computer code has been developed for calculating the forces acting on a heat exchanger tube, as well as the tube trajectory. A 0·6 m long (between modal node points) portion of a heat exchanger tube is modelled as a simple two-degree-of-freedom mass-spring system with a 0·24 kg mass (m_{yz}) and 69 N/mm spring stiffness (k_{yz}) in the Y and Z directions. A loose support is at mid-span. The differential equations describing the free motion of the tube can be expressed by

$$m_{yz}a_y + k_{yz}e_y = F_y, \qquad m_{yz}a_z + k_{yz}e_z = F_z. \tag{19}$$

For simplicity, damping along the tubing is neglected.

To solve for the tube motion and the support forces, the fourth order Runge–Kutta method is used for numerical integration. In the code, it is assumed that the differences in a_y and a_z between two consecutive time steps are not remarkable and have negligible feedback on F_y and F_z. The previous step's accelerations $a_y^{(n-1)}$, $a_z^{(n-1)}$ are used and the following explicit equations are solved in the Runge–Kutta integration calculations:

$$m_{yz}a_y^{(n)} + k_{yz}e_y^{(n)} = F_y(e_y^{(n)}, e_z^{(n)}; v_y^{(n)}, v_z^{(n)}; a_y^{(n-1)}, a_z^{(n-1)}),$$
$$m_{yz}a_z^{(n)} + k_{yz}e_z^{(n)} = F_z(e_y^{(n)}, e_z^{(n)}; v_y^{(n)}, v_z^{(n)}; a_y^{(n-1}, a_z^{(n-1)}. \quad (20)$$

In VIBIC, each node of the tube has six DOF even though only a two DOF squeeze film model has been presented. In order to implement the model into VIBIC, the test code has been extended to simulate the tube with six DOF. For the DOF other than the Y and Z directions, the squeeze film forces are assumed negligible and only an additional constant damping factor is applied for each DOF. (Rogers *et al*. [16] showed that rocking motions had negligible influence on lateral squeeze forces.) The masses and stiffnesses on each DOF are calculated based on a simply supported beam system. The general equation of the system for each DOF is

$$m_{dof}\ddot{U}_{dof} + c_{dof}\dot{U}_{dof} + k_{dof}U_{dof} = F_{dof}, \quad (21)$$

where *dof* can be any one of x, y, z, rx, ry, or rz which represent the X, Y and Z directions and rotations about X, Y and Z; F_{dof} is the external force (or moment) including squeeze film forces, solid contact forces (and moments) and excitation forces. The sticking/sliding friction algorithm developed by Tan and Rogers [14] has been merged into the test code.

4.3. VERIFICATION

It is difficult to confirm that the above models and the algorithm are acceptable and correct without any comparison and verification. Unfortunately, there are no experimental data to be compared with, and no literature can be used to validate these models directly. Therefore, numerical analyses and comparisons are conducted to verify the presented models and algorithms.

4.3.1. *System equivalent damping*

The system damping factor is one of the most important parameters in heat exchanger tube dynamics. Pettigrew *et al*. [20] have some experimental data on damping on liquids and give several semi-empirical expressions to formulate damping. However the simulated tube system in the test code has a very strong non-linear damping factor which comes from the squeeze film force. In order to compare this damping ratio with experimental data to see whether it is in the normal range of real system squeeze-film damping ratios, an equivalent damping ratio of this system is needed.

The equivalent damping ratio can be calculated from the frequency response of the simulated tube. Figure 6 shows two frequency response curves which are obtained by applying a 0·6 N exciting sine force to the tube system in the Z direction and varying the force frequency from 75 Hz to 95 Hz very slowly to allow the system to reach a steady response. The solid line is obtained with every squeeze film force term in F_{sqn} in equation (1) and the dashed line is calculated with only the damping term expressed by the first term; because the fluid inertia is taken away, the resonant frequency and the whole curve are moved to a slightly higher frequency area. This phenomenon coincides with theoretical expectations. The equivalent damping ratio is calculated by a linear system's governing equation:

$$\zeta \approx (\omega_2 - \omega_1)/2\omega_n, \quad (22)$$

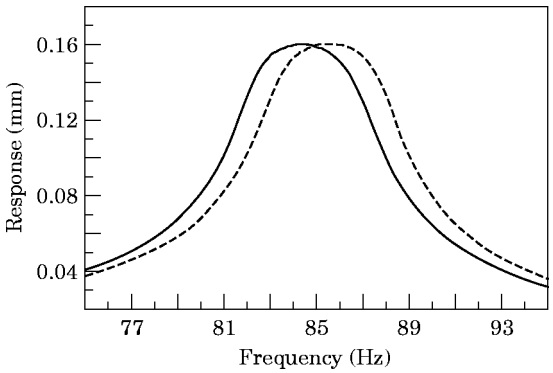

Figure 6. Frequency response of tube system: ——, damping and inertia; – – –, damping only.

where ω_n is the resonant frequency where the system reaches the largest response assuming $\zeta \ll 1$; ω_1 and ω_2 are the frequencies on either side of resonance where the system reaches 0·707 times the largest response. For the case shown in Figure 6, $\zeta = 0{\cdot}037$.

With this method, a series of simulations has been done by changing the amplitude of the exciting sine force. As seen in Figure 7, with increasing amplitude of the exciting force, the tube response increases but is restricted by the loose support. The damping ratio increases almost linearly with the excitation force; it is in the range of 0·7–6% which is comparable with the results obtained by Pettigrew *et al*. [20]. From the view of system equivalent damping, it is clear that the simulated system is comparable to a real system.

4.3.2. *Comparison with Larsson and Lundberg's work*

Larson and Lundberg [21] did some impact experiments of a roller on a lubricated surface and used a similar model as is described in section 3. The studies also involved squeeze film and solid forces for their lubrication research. Even though the objectives are not the same, comparisons are still useful.

Substituting the squeeze film model and parameters used by Larsson and Lundberg into the test code and keeping the algorithms described in previous sections, such as the Runge–Kutta integration method to solve for the tube motion and the Newton–Raphson iteration method to calculate the wall deflection, excellent results as shown in Figure 8 were achieved and which are almost identical to those Larsson and Lundberg obtained with

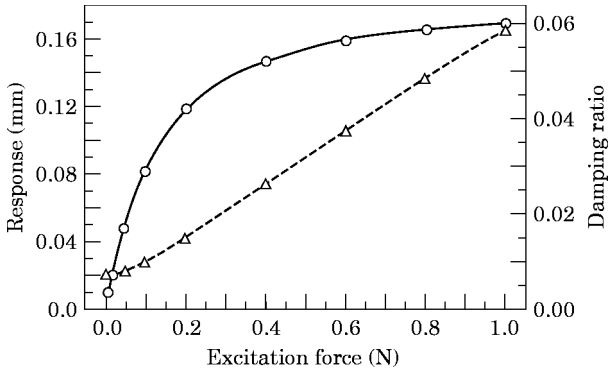

Figure 7. Force–response–damping relationship: —○—, response; – –△– –, damping ratio.

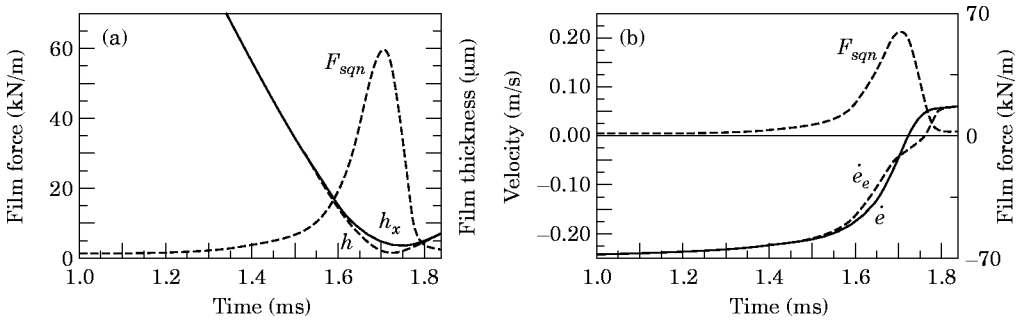

Figure 8. Reproduction of Larsson and Lundberg's work: (a) squeeze film force and film thicknesses as function of time during impact; (b) velocities of tube wall and tube centre during impact.

their own algorithms. From the comparison with Larsson and Lundberg's work, it can be seen that the test code algorithms work very well and are reliable.

4.4. MODEL MODIFICATION FOR FINITE WIDTH SUPPORTS

The forces expressed in equation (1) are for short length cylindrical squeeze films in which only the axial flow along the tube is considered and the circumferential flow is neglected. Therefore, equation (1) will over-estimate the squeeze forces in most real heat exchangers. Lu and Rogers [5] formulated a finite length cylindrical squeeze film model for 1-D diametrical motions (which has no centripetal and Coriolis inertia forces) as

$$F_{sqn} = -\frac{\mu L R^3}{C_r^2} L_{a1} \frac{12\pi}{\gamma^3} \dot{\varepsilon} - \rho L R^3 L_{a2} \frac{2\pi(1-\gamma)}{\varepsilon^2} \ddot{\varepsilon} - \rho L R^3 L_{a3} \frac{8\pi(1-\gamma)^2}{5\varepsilon^3\gamma} \dot{\varepsilon}^2, \tag{23}$$

where $L_{a(i)}$ $(i = 1, 3)$ are side leakage factors for each term and have the form $L_{a(i)} = 1 - \tanh(\lambda_{(i)} L/D)/(\lambda_{(i)} L/D)$.

The finite model is more accurate for calculating the squeeze film force in most real heat exchanges, but it cannot simulate arbitrary 2-D motions so that it has little practical value. A simple modification of the short model has been carried out by comparing the short model (1) with the finite model (23) under the same free motion conditions. Figure 9 shows one test case obtained for $L/D = 1$ with a set of typical heat exchanger parameters. The solid line is calculated from the short model and the dashed one from the finite model. The mean value of the ratio is then calculated to be 1·45. By changing L/D from 0 to 2·0,

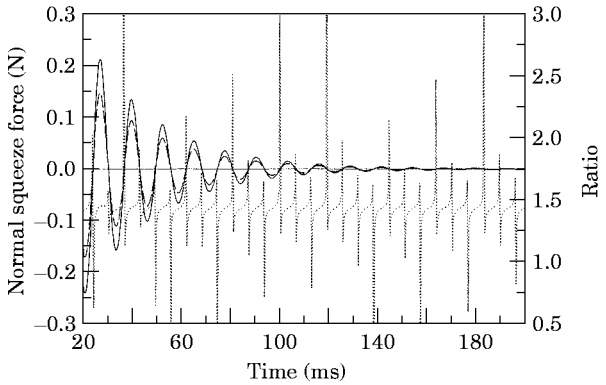

Figure 9. Comparison of short and finite width models: ——, short model; – – – –, finite model; · · · ·, ratio; $C_r = 0{\cdot}19$ mm, $e_z(0) = 0{\cdot}08$ mm, $F_z = 3$ N, $L/D = 1$.

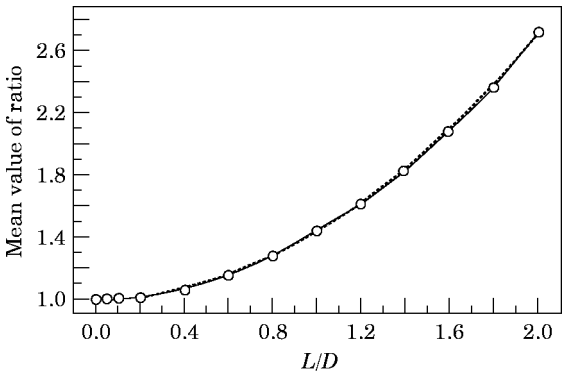

Figure 10. Modification factor for short width model: —○—, computational; · · · ·, $y = 1 + 0{\cdot}0037x + 0{\cdot}43x^2$.

Figure 10 is obtained in which the solid line shows the computational relationship between the mean value of force ratio and L/D; the dotted line is a quadratic regression equation which fits the computed result very well. Therefore, a modification factor can be expressed as

$$F_{mod} = 1/(1 + 0{\cdot}0037L/D + 0{\cdot}43(L/D)^2). \tag{24}$$

Simply adding this factor to equation (1) reduces the over-estimation of the squeeze factor.

4.5. IMPLEMENTATION INTO VIBIC

VIBIC is a computer software package written in FORTRAN which simulates the dynamic behaviour of a 3-D vibrating beam as it interacts with its loose supports. It was originally developed by Rogers and Pick [1, 2] and has been being improved from Version 1·0 in 1975 to the present Version 6·2 which has more than 6000 statements. The update from Version 6·0 to 6·1 (in 1994) included the work by Tan and Rogers [14] by implementing a new friction model which can simulate the sticking-slipping phenomenon between contacting surfaces. VIBIC now consists of two parts: Part 1 is called FREMOD (for natural frequencies and mode shapes) in which the beam (i.e., tube) is modelled using 3-D beam finite elements which include the effects of shear deformation and rotational inertia. The undamped natural frequencies and mode shapes are calculated using the RSG (EISPACK) eigen-solver. Part 2 is called VIBSIM (for vibration and impact simulation) in which the tube vibration and impacts against its supports are simulated by using a fourth order Runge–Kutta integration method and modal superposition. The modal basis excludes the effect of the loose supports since the support forces acting on the tube are calculated separately [22]. Finally, the wear work rate (normal forces multiplied by sliding velocity) is given by VIBSIM based on the impact history and contact forces in order to further analyse for wear damage.

Because the model described by equation (1) is only suitable for cylindrical squeeze films, the implementation of the test code is only for the circular support type even though VIBSIM accepts four types of support (circular hole, trilobed broached hole, scallop bars and flat bars). For non-circular support types, the squeeze film is not very strong [23]. As well, there are no suitable theoretical models for these types of squeeze film so that no squeeze film force is calculated for non-circular supports.

It was not very difficult to put the test code into VIBSIM since everything that the test code needed could be found easily in VIBSIM and vice versa. Two new subroutines named WALDEF, which mainly calculates the wall deflection, and SQZFOR, which calculates

the squeeze film forces, and one new function named FXW, which calculates equation (17), were reconstructed from the test code and interfaced with VIBSIM.

5. RESULTS AND DISCUSSION

This section will give some results for three simulation cases; two of them are from the test code and one is from VIBIC. All the results are obtained by using a typical set of heat exchanger parameters: $D = 15{\cdot}9$ mm, $C_r = 0{\cdot}19$ mm, $K = 16 \times 10^6$ N/m, $\mu_0 = 0{\cdot}4$, $\rho_i = \rho_d = 1000$ kg/m^3, $\mu = 0{\cdot}001$ Ns/m^2. L/D in the test code is set to be 0·5 due to the short length squeeze film model and in VIBIC it is 1·4 since the modified short model is used to fit a real situation. The constant time increment for numerical integration is set to a value in each case which is small enough so that there is no significant difference in the results if it is reduced more.

Case 1 shown in Figure 11 simulates a freely decaying orbital motion with two significant solid contacts based on the two-DOF system. The initial position is at $e_y^{(0)} = 0{\cdot}17$ mm, $e_z^{(0)} = 0$. In order to obtain a significant contact to show how the dynamic model and algorithms work, the initial velocity is set to be $v_y^{(0)} = 0$, $v_z^{(0)} = 0{\cdot}34$ m/s which is quite large and not physically reasonable. Therefore, the results shown in Figures 11(b) and (c) in

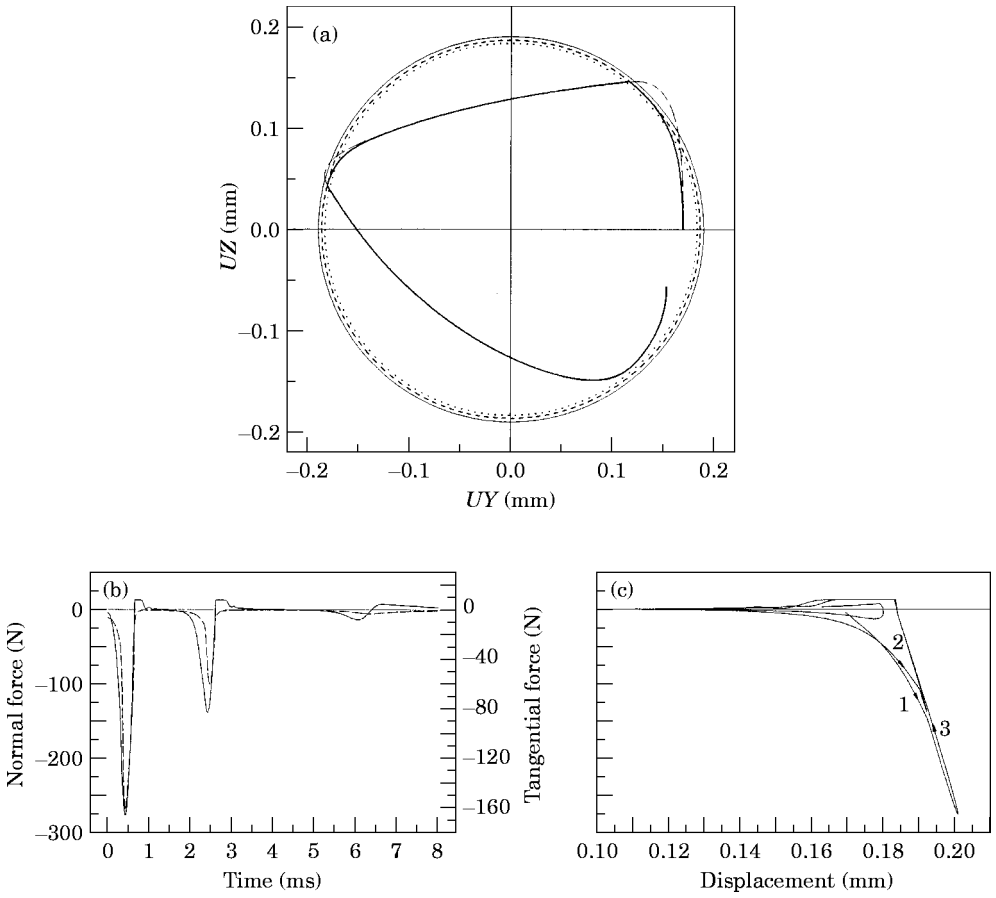

Figure 11. Free motion with solid contact. (a) Trajectory of tube: ——, clearance circle; - - - -, incline; ..., roughness; – – – –, tube centre; ——, tube wall. (b) Normal and tangential force history: ——, normal force; – – – –, tangential force. (c) Normal force as function of displacement.

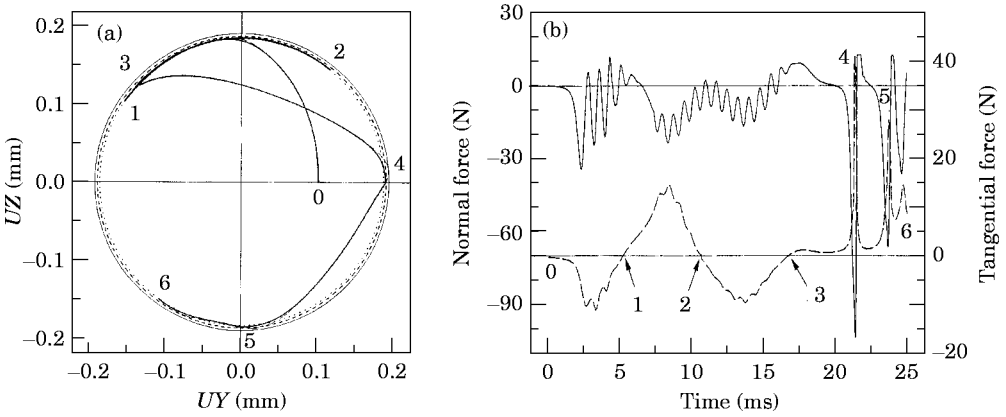

Figure 12. Forced motion with reversal. (a) Trajectory of tube: ——. clearance circle; - - -, incline; · · · ·, roughness; – – –, tube centre; ——, tube wall. (b) Normal and tangential force history: ——, normal force; – – –, tangential force.

which the maximum normal and tangential forces are about 280 N and 160 N, respectively, are large for a real heat exchanger. Figure 11(a) shows the trajectory of the tube. The radii of the three circles are C_r, $C_r - h_s$ and $C_r - h_s - h_r$, respectively. The dashed trajectory line represents the track of the tube centre while the solid line is the track of the "tube wall" (tube centre displacement minus wall deflection). The freely decaying orbit seems reasonable and indicates that the mass–spring model and Runge–Kutta method are working well. The deflections of the tube wall (i.e., the gap between the solid and dashed trajectory lines) are significant and seem credible which indicate that the dynamic model shown in Figure 5 and the Newton–Raphson iterating method are working well. Figure 11(b) shows the normal and tangential force histories corresponding to Figure 11(a). For the normal force shown by the solid line, positive values represent suction forces which are limited by the maximum suction F_{max} in equation (15). A negative normal force means either a squeeze force or a contact force. As seen, both the normal and tangential forces change reasonably smoothly during the transitions to and from solid contact. The normal force as function of the radial displacement is given by Figure 11(c) in which the arrows marked on the line indicate the direction of the tube motions. The squeeze force reaches approximately 65 N when the roughness zone is entered. Lines 1 and 2 show the two transition-to-solid-contact processes. The slope of the almost straight line 3 represents the tube–support contact stiffness K. Lines 1 and 2 blend smoothly with line 3 as required. The distances between lines 1 and 3 or lines 2 and 3 during contact are caused by the material damping. This figure shows that the transition and contact models work well.

Case 2 (Figure 12) shows the tube motions driven by two external sine forces along the Y and Z directions which are 10 N at 90 Hz and 20 N at 26 Hz, respectively. The initial condition is: $e_y^{(0)} = 0{\cdot}1$ mm, $e_z^{(0)} = 0$; $v_y^{(0)} = 0$, $v_z^{(0)} = 0{\cdot}1$ m/s. As shown in Figure 12(a), the motion begins at the initial position, point 0, and involves three reversals of sliding direction at points 1, 2 and 3 marked in sequence; two solid contacts occur at the points 4 and 5; the motion is stopped at point 6. Figure 12(b) shows the normal and tangential forces similarly to Figure 11(b). When the tube is pressed against its support wall and slips along the wall, sinusoidal bounces occur as shown by the solid line (normal force history). The numbers marked on the dashed line (tangential force history) correspond to the points marked in Figure 12(a) and clearly show reversals in sliding direction. Reversals 1 and 3 occur in the fully squeeze zone so that the tangential force changes smoothly from negative

to positive. Reversal 2 happens in the transition zone so that part of the solid friction is counted in the total tangential force and causes the small jump at point 2.

Figure 13 (Case 3) is obtained from VIBIC for a finite element model in which a 0·6 m long piece of tube is modelled as 20 equal length beam elements with a loose support at the middle (i.e., the 11th node) and two flexible no-clearance supports at the ends (i.e., the first and 21st nodes). Two DOF, x and rx, are constrained for the whole tube; they could be included but result in high frequency oscillations. The y and z DOF are constrained additionally at the ends. Therefore, there are 80 kept DOF (i.e., equations left after rigid constraints are removed) in the finite element model. Fourteen modes are included in the simulation (i.e., seven in each plane).

Case 3 is a "mostly" free motion case with three solid contacts. "Mostly" is used because in the beginning of the motion, the tube is driven at node 6 by two external forces in the Y and Z directions for 0·18 cycle to obtain a large enough velocity (the initial motion parameters are all zero). The rest of the motion is free. For the same reason as in Case 1, in order to obtain several significant contacts to see how the transition model works, the external forces are set to be a 200 N, 100 Hz cosine force on Y and a -600 N, 400 Hz sine force on Z which are large for a real heat exchanger. As well, the forces in Figure 13(b) also have very large peak values. However, this case shows nicely that VIBIC works very well with the new implementations. The tube trajectory at node 11 where the support is located is shown in Figure 13(a). Similar to Case 1, the tube is involved in three significant solid contacts and is deflected heavily during the transitions to contacts. The trajectory after half way to the end seems strange and not like free motion but it is. The reason is that the tube in VIBIC is modelled as a finite element model rather than the mass–spring system in the test code so that high frequency modes exist and are excited by the severe contacts. As well, the forces in the Y and Z directions are quite different so that the mode shapes excited by the forces are different too. These cause the strange tube trajectory. Figure 13(b) shows the normal (solid line) and tangential (dashed line) forces acting on node 11. The forces vary smoothly during the transitions to and from solid contacts and the positive normal force is limited by the maximum suction force as expected.

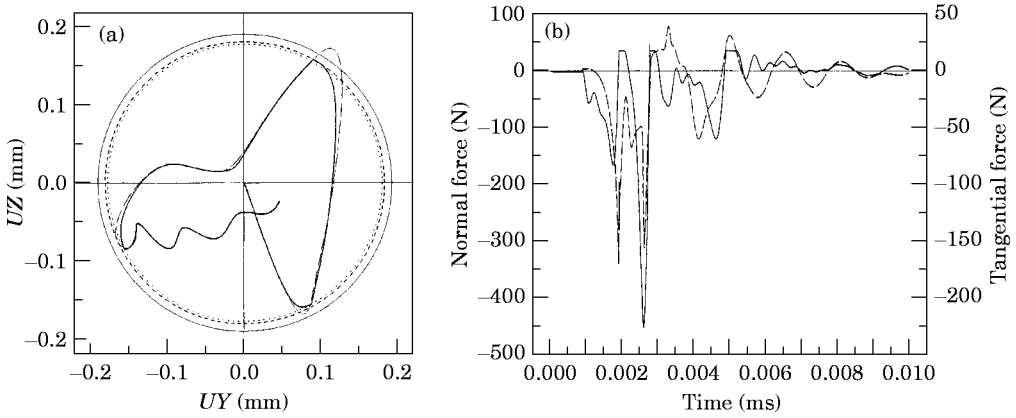

Figure 13. VIBIC Result: free motion with solid contact. (a) Trajectory of tube: ——, clearance circle; - - -, incline; · · · ·, roughness; – – –, tube centre; ——, tube wall. (b) Normal and tangential force history: ——, normal force; – – –. tangential force.

6. CONCLUSIONS

A simplified two-dimensional model for a cylindrical squeeze film with transitions to and from solid contact has been developed which includes an estimation of the tube/support deflection and approximates the effects of the surface roughness and tube/support inclination. A simple function of support length (width) to tube diameter is used to adapt the short length squeeze film formulation to finite length applications.

Large amplitude and arbitrary tube motions have been simulated by a test code which has been developed based on the models and algorithms. A new friction model with six-DOF motion has been merged into the test code. Numerical analyses and simulations have been done which show that the models and algorithms appear to work well. The test code has been implemented into VIBIC after verification and modification.

The simulation results for three typical tube motion cases have been investigated; two cases are obtained from the test code and one is from the new version of VIBIC. The results give reasonable large amplitude tube trajectories and squeeze/contact forces which are based on the values of the instantaneous kinematic variables. The dynamic transition model works very well and the transitions to and from solid contact are reasonably smooth.

ACKNOWLEDGMENTS

The work reported here was supported by Atomic Energy of Canada Limited as part of its work on heat exchanger tube vibration and wear prediction. The authors also wish to acknowledge the support of the Natural Sciences and Engineering Research Council of Canada and the University of New Brunswick.

REFERENCES

1. R. J. Rogers and R. J. Pick 1976 *Nuclear Engineering and Design* **36**, 81–90. On the dynamic spatial response of a heat exchanger tube with intermittent baffle contacts.
2. R. J. Rogers and R. J. Pick 1977 *Nuclear Engineering and Design* **44**, 247–252. Factors associated with support plate forces due to heat exchanger tube vibratory contact.
3. L. San Andres and J. M. Vance 1987 *ASLE Transactions* **30**, 69–76. Force coefficients for open-ended squeeze-film dampers executing small-amplitude motions about an off-centre equilibrium position.
4. L. San Andres 1985 *Ph.D. Dissertation*, *Department of Mechanical Engineering*, *Texas A and M University*. Effects of fluid inertia on squeeze film damper force response.
5. Y. Lu and R. J. Rogers 1994 *ASME Journal of Tribology* **116**, 588–596. Normal instantaneous squeeze film force for a finite length cylinder.
6. A. El-Shafei and S. H. Crandall 1991 *ASME Rotating Machinery and Vehicle Dynamics DE* **35**, 219–228. Fluid inertia forces in squeeze film dampers.
7. Y. Lu and R. J. Rogers 1995 *Journal of Fluids and Structures* **9**, 835–860. Instantaneous squeeze film force between a heat exchanger tube with arbitrary tube motion and a support plate.
8. S. Dubowsky and F. Freudenstein 1971 *ASME Journal of Engineering for Industry* **93**, 305–316. Dynamic analysis of mechanical systems with clearances: Parts 1 and 2.
9. K. H. Hunt and F. R. E. Crossley 1975 *ASME Journal of Applied Mechanics* **42**, 440–445. Coefficient of restitution interpreted as damping in vibroimpact.
10. W. R. Chang and F. F. Ling 1992 *ASME Journal of Tribology* **114**, 439–447. Normal impact model of rough surfaces.
11. A. D. Lewis and R. J. Rogers 1988 *Journal of Sound and Vibration* **125**, 403–412. Experimental and numerical study of forces during oblique impact.
12. R. J. Rogers and A. D. Lewis 1990 *Journal of Sound and Vibration* **141**, 507–510. Further numerical studies of oblique elastic impact.
13. X. Tan and R. J. Rogers 1996 tent. accepted by *ASME Journal of Dynamic Systems*, *Measurement and Control*. Simulation of friction in multi-degree-of-freedom vibration systems.

14. X. TAN and R. J. ROGERS 1996 *Joint ASME PVP/ICPVT-8 Conference*, *July* 21–26, *Montreal*, *Flow-Induced Vibration*, 347–358. Dynamic friction modelling in heat exchanger tube sytems.
15. W. GOLDSMITH 1960 *Impact*: *The Theory and Physical Behaviour of Colliding Solids*. London: Edward Arnold; see p. 258.
16. R. J. ROGERS, M. M. BERG, W. H. S. RAMPEN, Y. T. SOH, H. M. TEU and T. K. V. TIN KIN WANG 1990 *Journal of Fluids and Structures* **4**, 583–603. Harmonic modelling of nonlinear fluid forces in finite length cylindrical squeeze films.
17. A. D. DEUTSCHMAN, W. J. MICHELS and C. E. WILSON 1975 *Machine Design—Theory and Practice*; Macmillan; see pages 211–213.
18. J. T. ODEN and J. A. C. MARTINS 1985 *Computer Methods in Applied Mechanics and Engineering* **52**, 527–634. Models and computational methods for dynamic friction phenomena.
19. C. P. KU and J. A. TICHY 1990 *ASME Journal of Tribology* **112**, 725–733. An experimental and theoretical study of cavitation in a finite submerged squeeze film damper.
20. M. J. PETTIGREW, R. J. ROGERS and F. AXISA 1986 *Flow-Induced Vibration ASME Pressure Vessels and Piping Conference*, *Chicago*, 89–98. Damping of multispan heat exchanger tubes: Part 2: in liquids.
21. R. LARSSON and J. LUNDBERG 1994 *Wear* **173**, 85–94. A simplified solution to the combined squeeze-sliding lubrication problem.
22. H. G. DAVIES and R. J. ROGERS 1979 *Journal of Sound and Vibration* **63**, 437–447. The vibration of structures elastically constrained at discrete points.
23. R, J. ROGERS, Y. HAN and Y. LU 1994 *Proceedings of the* 12*th Symposium on Engineering Applications of Mechanics—Interaction of Fluids*, *Structures and Mechanisms*, 93–102. Heat exchanger squeeze film forces for tri-lobe broached hole supports.
24. T. ZHOU and R. J. ROGERS 1996 *Joint ASME/ICPVT-8 Conference*, *July* 21–26, Montreal, *Flow-Induced Vibration*, 257–270. Simulation of two-dimensional squeeze film and solid contact forces acting on a heat exchanger tube.
25. R. J. ROGERS and G. C. ANDREWS 1977 *ASME Journal of Engineering for Industry* **99**, 131–137. Dynamic simulation of planar mechanical systems with lubricated bearing clearances using Vector–Network Methods.

APPENDIX: NOMENCLATURE

a_y, a_z	accelerations of tube along Y and Z directions.
a_n, a_t	accelerations of tube along normal and tangential directions, $a_n = \ddot{e} - e\dot{\Psi}^2$, $a_t = e\ddot{\Psi} + 2\dot{e}\dot{\Psi}$.
C_r	radial clearance between tube and support, $C_r = R - r$.
c_{dof}	coefficients of viscous damping for each DOF.
D	diameter of support hole, $D = 2R$.
e_y, e_z	displacements of tube centre along Y and Z directions.
e, $\dot{e}$, $\ddot{e}$	instantaneous radial displacement of tube centre and derivatives with respect to time.
F_{ctn}, F_{ctt}	contact forces in normal and tangential directions.
F_{dof}	projections of resultant force on each DOF.
F_{max}	maximum suction force.
F_{mod}	modification factor.
F_n, F_t	projections of resultant force on normal and tangential directions.
F_{sqn}, F_{sqt}	squeeze film forces in normal and tangential directions.
h_x	minimum film thickness that considers deflection, $h_x = C_r - e + X_w$.
K	tube/support combined stiffness.
k_{dof}	stiffnesses of beam system for each DOF.
L	support width.
m_{dof}	masses of beam system for each DOF.
R, r	support hole and tube radii.
U_{dof}, $\dot{U}_{dof}$, $\ddot{U}_{dof}$	displacements for each DOf and their derivatives.
v_y, v_z	tube velocities along Y and Z directions.
v_n, v_t	tube velocities along normal and tangential directions, $v_n = \dot{e}$, $v_t = e\dot{\Psi}$.
γ	$(1 - \varepsilon^2)^{1/2}$.
λ_1, λ_2, λ_3	Solution eigenvalues of side-leakage factors. $\lambda_1 = \sqrt{(1 + 2\varepsilon^2)}/\gamma$, $\lambda_2 = 1/\sqrt{\gamma}$, $\lambda_3 = \sqrt{\dfrac{9(2\gamma^3 - 2 + 3\varepsilon^2)/}{8\gamma^2(1 - \gamma)^2}}$

$\varepsilon, \dot{\varepsilon}, \ddot{\varepsilon}$	Instantaneous eccentricity and its derivatives, $\varepsilon = e/C_r$ or $\varepsilon = (e - X_w)/C_r$.
μ	Absolute fluid viscosity.
μ_k, μ_0	Kinetic friction coefficient and plateau friction during impact.
ρ	Fluid density.
$\Psi, \dot{\Psi}, \ddot{\Psi}$	Instantaneous angular displacement and its derivatives.